

# Computational design of a pH-sensitive IgG binding protein

Eva-Maria Strauch<sup>a</sup>, Sarel J. Fleishman<sup>a,1</sup>, and David Baker<sup>a,b,2</sup>

<sup>a</sup>Department of Biochemistry and <sup>b</sup>Howard Hughes Medical Institute, University of Washington, Seattle, WA 98195

Edited by James A. Wells, University of California, San Francisco, CA, and approved December 4, 2013 (received for review July 18, 2013)

Computational design provides the opportunity to program protein–protein interactions for desired applications. We used de novo protein interface design to generate a pH-dependent Fc domain binding protein that buries immunoglobulin G (IgG) His-433. Using next-generation sequencing of naïve and selected pools of a library of design variants, we generated a molecular footprint of the designed binding surface, confirming the binding mode and guiding further optimization of the balance between affinity and pH sensitivity. In biolayer interferometry experiments, the optimized design binds IgG with a  $K_d$  of ~4 nM at pH 8.2, and approximately 500-fold more weakly at pH 5.5. The protein is extremely stable, heat-resistant and highly expressed in bacteria, and allows pH-based control of binding for IgG affinity purification and diagnostic devices.

computational interface design | pH-sensitivity | antibody purification

Recombinant monoclonal antibodies and Fc-fusion proteins have become an important class of biological pharmaceuticals and are widely used as research reagents. Their manufacture typically involves mammalian cells as the expression host and affinity chromatography as a key purification step. Although cell-line development and engineering have significantly enhanced antibody yields, the downstream purification steps remain expensive and reduce productivity. Most antibody purification pipelines use a Protein A-based purification step, which contributes to the majority of the raw-material costs (1, 2). Antibody elution from a Protein A column is typically achieved by lowering the pH to 3. However, at such low pH, aggregation and denaturation of the antibody and of Fc-fusion proteins often occur (3–6), resulting in reduced yields (7).

pH-dependent binding occurs if protonation of an ionizable residue, such as histidine, shifts the binding equilibrium. Previous efforts to engineer pH-dependent protein switches have either used structure-guided insertion of ionizable groups (8) or systematic histidine scanning mutagenesis (9, 10). These approaches often result in lower affinity interactions or low sensitivity to physiologically relevant pH changes. Computational interface design potentially provides a way to address this challenge by introducing structural elements that interact favorably with an ionizable group on the surface of the target protein in one ionization state, but not the other. Our recently reported hotspot-based design strategy starts by computing idealized core interaction sites (“hotspots”) and then scans a large set of scaffold proteins for surfaces that can present the hotspots and form stabilizing interactions with the target site (11). Here, we describe the adaption of this methodology to generate pH-sensitive binding proteins.

## Results

**Computational Design.** Despite differences in overall topology, several previously characterized Fc binding proteins interact with the same “consensus” region between the CH2 and CH3 domain (Fig. 1*A* and *E*). There is remarkable convergence in the contact residues both naturally occurring and randomly selected proteins and peptides use to bind to this region (Fig. 1*A*). We sought to

utilize some of these crucial hotspot interactions to generate IgG binding proteins with pH-dependent binding functionality.

Inspection of the binding interface on Fc reveals two accessible histidine residues, His-310 and His-433 (human IgG1 numbering). Of the two, His-433 is considerably more surface exposed. With the assumption that the burial of a surface exposed histidine residue would lead to pH sensitivity close to physiological pH (12), we set out to design a protein that binds to the Fc consensus region and buries one of the accessible histidine residues. We applied hotspot-guided protein interface design (11, 13), and aimed to generate interactions with and around Fc His-433 or His-310 to achieve pH-dependent binding. We started by generating ensembles of disembodied interaction hotspot residues based on Gln-11, Phe-14, and Leu-18 from minimized Protein A (14) (Fig. 1*B* and *C* and Fig. S1). We also considered tryptophan in place of Phe-14 (Fig. 1*B* and *D*) and asparagine in place of Gln-11. Alternative rotameric states, not clashing with the target, were included for asparagine, glutamine, and leucine (Fig. 1*C* and Fig. S1) to provide more solutions for scaffold placement onto the precomputed hotspot residues. We then searched for protein scaffolds with high bacterial expression and solubility that could host the hotspot residues in the correct relative orientations. After successful placement of the hotspot residues (*Methods*), the remainder of the interface was redesigned by using RosettaDesign (15, 16) and designs were filtered and ranked based on computed binding energy and shape complementarity (*Methods*).

**Experimental Characterization of Binding and Binding Mode.** Seventeen designed proteins (Table S1) were expressed on the surface of yeast and binding was assessed by flow cytometry following incubation with 700 nM biotinylated human IgG1 (Rituxan) that had been fluorescently labeled and oligomerized through binding to streptavidin-phycoerythrin (PE). Nine designs had detectable binding signals. The strongest signal was observed for design FcB6, which was designed to hydrogen bond to both Asn-434 and

## Significance

Protein–protein interactions are part of almost every biological process; hence, the ability to manipulate and design protein binding has widespread applications. Here, we describe an approach to designing pH-dependent protein interfaces and use it to design a protein that binds antibodies at high pH but poorly at low pH. The designed protein should be useful for antibody affinity purification and diagnostic devices.

Author contributions: E.-M.S., S.J.F., and D.B. designed research; E.-M.S. and S.J.F. performed research; E.-M.S. and S.J.F. contributed new reagents/analytic tools; E.-M.S., S.J.F., and D.B. analyzed data; and E.-M.S. and D.B. wrote the paper.

Conflict of interest statement: The University of Washington has filed a patent on the Fc binding protein and its variants.

This article is a PNAS Direct Submission.

<sup>1</sup>Present address: Department of Biological Chemistry, Weizmann Institute of Science, Rehovot 76100, Israel.

<sup>2</sup>To whom correspondence should be addressed. E-mail: dabaker@uw.edu.

This article contains supporting information online at [www.pnas.org/lookup/suppl/doi:10.1073/pnas.1313605111/-DCSupplemental](http://www.pnas.org/lookup/suppl/doi:10.1073/pnas.1313605111/-DCSupplemental).

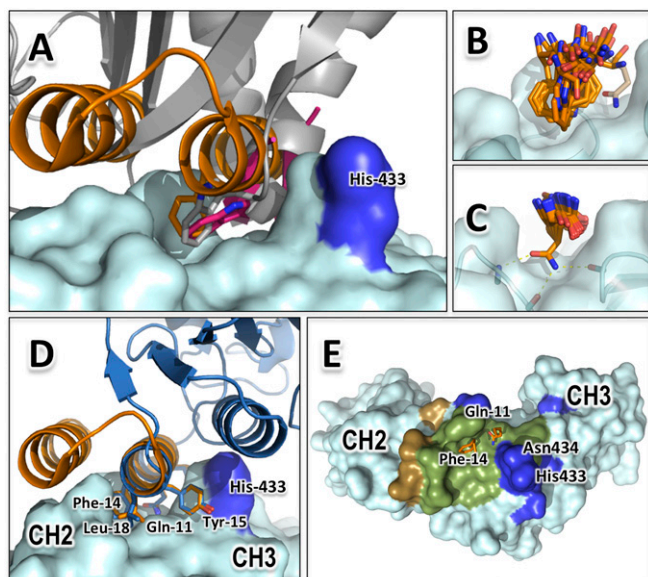


**Fig. 1.** Design strategy. (A) Convergent solutions to Fc binding: The phenyl ring of Phe-14 in Protein A [orange; Protein Data Bank (PDB) ID code 1L6X] occupies the same position as the indole ring of Trp-133 of the neonatal Fc receptor (FcRn; PDB ID code 1I1A, gray) (29) and Trp-11 of the synthetic peptide isolated through phage display (pink, PDB ID code 1DN2) (14). (B and C) Diversified hotspot ensembles of Phe-14 (B) and Gln-11 (C). (D) Comparison of minimized Protein A B-domain (Z34C) (orange) to model of FcB6 bound to the Fc region of IgG1. The two structures have helices on opposite sides of the primary binding epitope. (E) Surface representation of the Fc domain. Green indicates the consensus-binding site where Protein A and other characterized binders interact. Brown indicates peripheral contacts by Protein A; blue residues buried by the new IgG binding protein FcB6. Some of the starting points for the de novo design protocol (disembodied Gln-11 and Phe-14 residues from Protein A) are indicated in orange.

His-433, and was thus an excellent candidate to optimize for pH-dependent binding. Both Protein A and FcB6 present a helix for binding between the CH2 and CH3 domain, and the core interface residues on FcB6, Q164, F167, Y168, M161, and L171 form very similar atomic contacts with Fc (Fig. 1D). However, no other amino acid is identical, and FcB6 differs substantially in binding mode from Protein A, because most of its additional contacts are with the CH3 domain and not with CH2. The scaffold on which FcB6 is based, pyrazinamidase from *Pyrococcus horikoshii* (17), does not bind Fc (Fig. S2), suggesting that the designed surface mediates binding. Competition with Protein A completely blocked binding of FcB6 to IgG1 (Fig. S2), indicating that the designed protein binds to the intended site on Fc.

**Binding Fitness Landscape.** To confirm the designed binding mode and identify possible avenues for improving the computational design, we used PCR mutagenesis in concert with one round of fluorescent-activated cell sorting (FACS) and next-generation sequencing, resulting in a fine-resolution map of the sequence-function landscape (18, 19). Sequencing of the C-terminal 51 positions, which contain the designed binding site, was carried out before and after selection for IgG binding. Fig. 2A shows the logarithm of the ratio of the frequency of observations of each substitution in the selected population to those in the unselected population; yellow-orange colors indicate substitutions enriched in the binding population, and green-blue colors are substitutions depleted in the binding population. The core residues, S134, Q164, F167, and Y168, at the designed interface with Fc are highly conserved (all substitutions are depleted). The two positions at which substitutions most increase binding are A135 and

E138; these residues were clearly far from optimal in the computational design. Mutations at these positions were also identified as consensus after three rounds of sorting and conventional sequencing (Fig. 2 and Fig. S3). Several substitutions, which were enriched in the first sort, such as L171W, were depleted in subsequent more stringent selections (Fig. S4).

**Optimization of pH-Dependent Binding.** To further optimize the balance between affinity and the pH dependence of binding, we constructed a library guided by the deep-sequencing data and Rosetta energy calculations and carried out rounds of selection for increased binding affinity at pH 6.5 and 8 (Fig. S5). In the library, a single core substitution L166F was introduced; S124 and A165 were allowed to be either alanine or serine; and E135, A138, K170, E160, and M161 were allowed to be any of the 20 amino acids (Fig. S6). Six selected variants after four rounds of sorting were tested for binding at pH 6.5 and pH 8. The variant with the greatest pH dependence (six- to sevenfold greater signal at pH 8 than pH 6.5 when expressed on the yeast surface) was subjected to more detailed analysis and will be referred to as FcB6.1. FcB6.1 contains the substitution E138V and an additional positive charge, A135R, at the binding surface (Fig. 3A–C). Structural modeling of the designed variant shows a tight fit around Fc His-433 (Fig. 3A): V138 makes van der Waals interactions with and shields His-433 from solvent, strengthening the hydrogen bond (20) between Ser-134 of FcB6.1 and His-433. R135 covers and packs against Fc His-433 from the other side and also interacts favorably with the close-by negatively charged surface on Fc (Fig. 3B). Protonation of Fc His-433 would considerably reduce binding affinity by increasing the cost of desolvating of this now-charged residue, eliminating the buried hydrogen bond to Ser134 (Fig. 3A) and introducing charge repulsion with R135 (Fig. 3C). The FcB6.1 variant contains several additional mutations including M161F, which increases the buried hydrophobic surface area at the interface and reduces the identity with Protein A to only four residues, and E160T, which reduces the negative charge projected toward CH3.

**Characterization of FcB6.1.** Protein production yields and stability are important properties of potential affinity reagents. FcB6.1 expresses well in *Escherichia coli*, yielding around ~60–70 mg/L in shake flasks without any optimization. CD spectroscopy showed that the protein is extremely stable; it remains folded at 80 °C (Fig. S7C; the scaffold is from a hyperthermophile), in 3 M urea, and in 1.5 M guanidine (Fig. S7A and B) FcB6.1 can be readily obtained in nearly pure form by heating bacteria to 80 °C for 20 min followed by centrifugation; indeed, we used this protocol for purifying the protein (Methods). Repetitive heating cycles up to 80 °C did not denature the protein (Fig. S7D). The heat stability is an attractive feature for an antibody capturing reagent for chip- or bead-based assays and diagnostics: Surfaces coated with FcB6.1 for antibody immobilization could be regenerated for reuse with different antibodies by a simple heating procedure, denaturant wash, or pH change.

To examine the specificity of FcB6.1, we measured binding to biotinylated human IgG from different subclasses and species via yeast surface display. Binding of the IgGs to the minimized Protein A variant (21) (miniA) was measured for comparison. As expected, FcB6.1 binds tightly to human IgG2, IgG4, and IgG1, slightly better than the miniA (Fig. S8) and comparably to mouse IgG1 and IgG2a (Fig. S8). FcB6.1 only binds weakly to IgG3 (which Protein A does not bind) and does not bind to rat IgG2a (Fig. S8).

We used ELISA and biolayer interferometry to determine the binding behavior of FcB6.1 to biotinylated IgG. For ELISA, purified FcB6.1 protein was immobilized and fitting of resulting absorption values yielded a  $K_d$  of 3.4 ( $\pm$  0.4) nM at pH 8.2 (Fig. 3D). At pH 5.5, the signal continued to increase at IgG

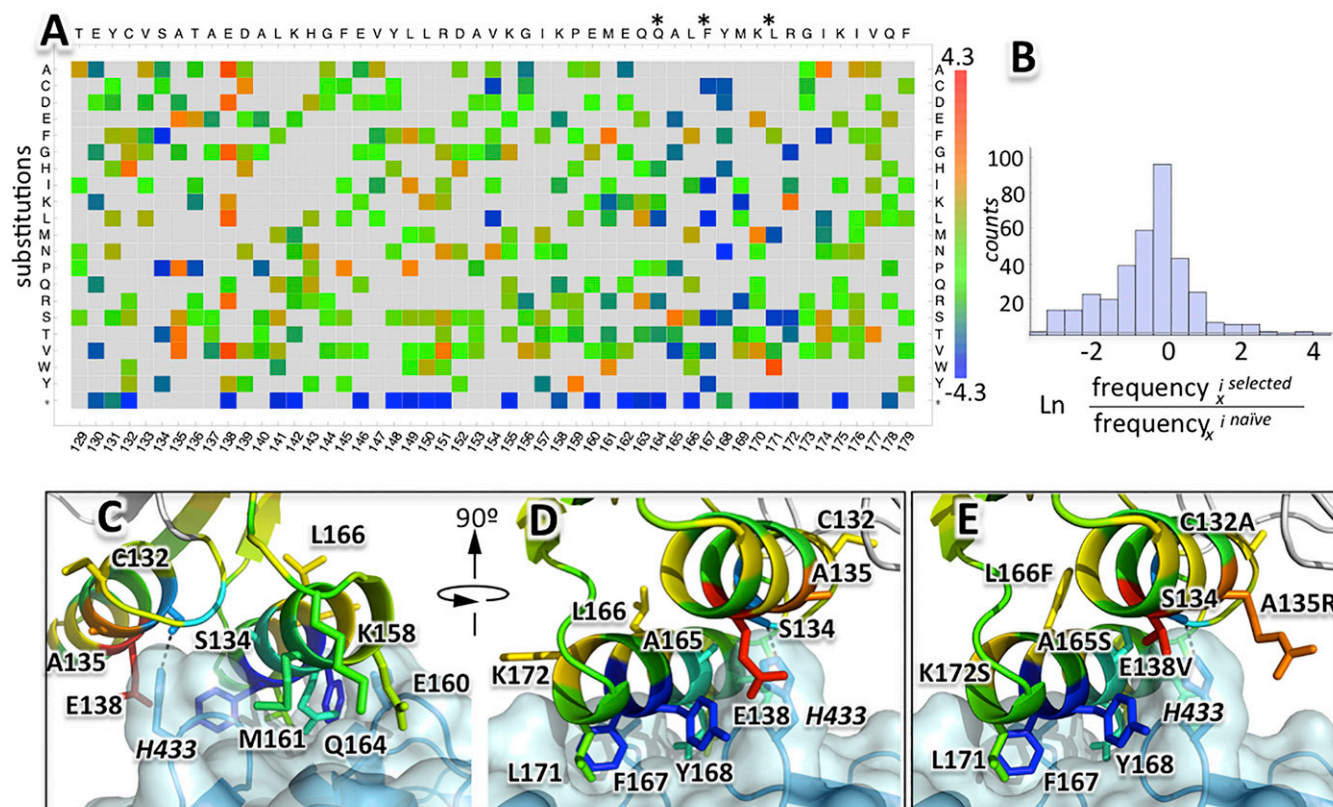


**Fig. 2.** Binding fitness landscape. For each substitution at each position, the natural log of the ratio between the frequency of the substitution in the population following selection for IgG binding and the frequency of the substitution in the unselected populations was computed. (A) Heat map of the log enrichment values for substitutions to each of the 20 aa (vertical axis) at each position (horizontal axis). The original designed sequence is shown at the top. Red, enrichment; blue, depletion following selection; gray, this substitution was not present in either pool. The core hotspot residues Phe167, Gln164, and Leu171 are marked with an asterisk. (B) Histogram of log enrichment ratios. (C and D) The optimality of the designed sequence mapped onto the FcB6 design model: Blue, mutations away from designed sequence are depleted, indicating that the designed residue is close to optimal; mutations away from the designed sequence are allowed (yellow) or favored (orange-red); green, neutral. Optimality was assessed by using a positional z score:  $z = (x - u)/s$ , where  $x$  is the log enrichment value of particular substitution,  $u$  is the log enrichment value of the designed residue at the position, and  $s$  is the SD of all enrichment values within the sequenced C-terminal part. (E) Model of the improved variant FcB6.1 colored by the optimality score obtained from the PCR mutagenesis library selections and sequencing described in A–D; the identified E138V and A135R substitutions are at positions that were far from optimal in the original design.

concentrations above 1  $\mu\text{M}$ , suggesting a  $K_d > 1 \mu\text{M}$ . For an independent estimate of the dissociation constant at pH 5.5 and pH 8.2, biotinylated IgG was immobilized onto Octet streptavidin-coated sensors and then incubated with FcB6.1. The pH dependence of the response after a 300-s association period was qualitatively similar to the ELISA results with much stronger binding at pH 8.2 than pH 5.5 (Fig. 3E). Very little difference in Protein A binding to the immobilized IgG for the two pH values was observed (Fig. 3E), indicating that the conformation of the binding site on IgG is not altered. Global fitting of the association and dissociation traces required a bivalent ligand model, suggesting that the two binding sites on the IgG may be coupled. Fitting of four independent titrations at each pH value (Fig. 3F) yielded averaged dissociation constants of  $4.0 \pm 2.5 \text{ nM}$  at pH 8.2 and  $3.78 \pm 3.2 \mu\text{M}$  at the lower pH value; the two fitted  $K_d$  values and amplitudes at pH 8.2 are  $4.0 \pm 2.5 \text{ nM}$  (~95%) and  $13.9 \pm 1.3 \text{ nM}$  (~5%), and at pH 5.5,  $5.8 \pm 1.7 \mu\text{M}$  (~70%) and  $1.7 \pm 0.2 \mu\text{M}$  (30%). Thus, immobilized to the biosensor surface, there is at least ~500-fold difference in binding affinity between pH 5.5 and pH 8.2, very favorable characteristics for pH-dependent chromatography.

To test whether FcB6.1 could serve for affinity purification of IgG molecules, we added a C-terminal cysteine residue accompanied

by a short glycine serine linker to couple the protein site specifically to a resin (SulfoLink; Thermo Scientific). To simulate a possible purification scenario, we spiked an IgG mix (20  $\mu\text{g}$ ; Innovative Research) into the supernatant of Freestyle 293 suspension cell culture and incubated it with FcB6.1cys-coated resin (Methods). Almost complete elution was achieved by dropping the pH to 5.5 to ensure complete protonation of His-433 and increasing the salt concentration to 500 mM (Fig. 4). Compared with Protein A, the FcB6.1cys resin allows much milder conditions for elution, which could be crucial for purification yields of acid labile antibodies that tend to aggregate and Fc-fusion constructs.

## Discussion

We have demonstrated that computational protein design can be used to generate affinity reagents with conditional binding functionality. In biolayer interferometry experiments, FcB6.1 binds the Fc hinge region of the IgG molecule approximately 500-fold more tightly at pH 8.2 than at pH 5.5. In addition to affinity purification and antibody immobilization on sensors, pH-dependent binding could be useful for selective release of cargo in the acidic environment of the endosome of cells targeted by a surface receptor-specific antibody.

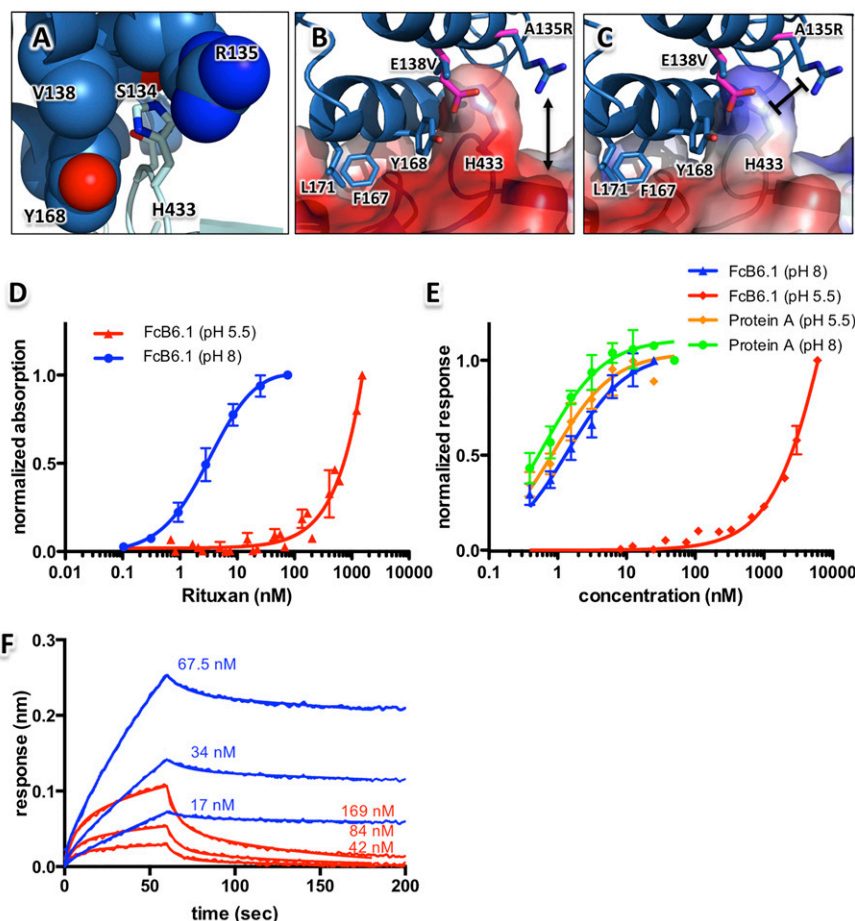


**Fig. 3.** pH-dependent binding. (A) Model of the optimized binding pocket around IgG His-433: His-433 forms a buried hydrogen bond to Ser-134 of FcB6.1 and is shielded from solvent by R135 and V138. Upon pH drop, His-433 becomes protonated, destroying the hydrogen bond and introducing a positive charge. The Poisson–Boltzmann electrostatic surface potential changes considerably from the nonprotonated (B) to the protonated (C) state, and whereas R135 can favorably interact with the highly negative surface (double-headed arrow) surrounding His-433, it introduces charge repulsion between His-433 and R135 of FcB6.1. Optimized model of FcB6.1 are in blue; original designed residues are in pink. (D) ELISA titrations of immobilized FcB6.1 with biotinylated Rituxan (E) bi-layer interferometry titrations responses of FcB6.1 or Protein A to immobilized Rituxan after a 300-s association period at the indicated pH. Binding of Protein A to IgG at the two pH values does not vary, suggesting that the conformation of the immobilized IgG is likely not affected by the pH change. (F) Association and dissociation sensograms with global fits to a bivalent ligand model of FcB6.1 binding to the immobilized ligand Rituxan at pH 8.2 (blue) and pH 5.5 (red) at indicated concentrations.

## Methods

**Computational Methods.** Disembodied hotspot residues Gln11, Phe14, and Leu18 from the minimized Protein A structure (1L6X) were subjected to small rigid-body perturbations against the Fc surface to generate “hotspot libraries” (Fig. 1 B and C and Fig. S1) and for the glutamine and leucine residues, additional inverse rotameric conformations were computed to give more alternatives for scaffold backbone placement (Fig. 1C). In addition, tryptophan residues were docked at the Phe14 site and asparagine residues at the Gln11 site. In parallel, 865 native scaffolds (11) were docked against Fc by PatchDock (22) constrained to bury Ile253, Met252, Met428, or Tyr436 using the “knob” feature. For each of the top 100 docked conformations, the capability to hold the hotspot residues as in the hotspot libraries was assessed similarly as previously described by using RosettaScripts (11, 13, 16) protocols Fc-2stubs.xml and Fc-3stubs.xml (SI Appendix). Three sets of hotspots were considered: a two-hotspot solution with Gln/Asn and Phe/Trp, and three-hotspot solution with Gln/Asn, Phe/Trp, and Leu disembodied residue libraries. The remainder of the sequence for each hotspot placement on a scaffold was optimized for high affinity binding to Fc, and the resulting designs were filtered and ranked based on computed binding energy ( $< -10$ ) and shape complementarity (23) ( $> 0.63$ ) calculated by the CCP4 package v.6.0.2 (24). Mutations that did not increase the predicted binding affinities were reverted back to their native identity.

Beneficial mutations identified via yeast binding selections were modeled using FoldIt (25). Mutations were introduced, followed by a repacking and

minimization step. Poisson Boltzmann electrostatic surface models for PyMol-based figures were computed through APBS (26), using either a protonated or deprotonated histidine 433 and a dielectric constant of 4.

**Antibody Biotinylation.** All antibodies were biotinylated by using SoluLink’s biotinylation kit as instructed by the manufacturer.

**Initial Design Evaluation and Yeast Surface Titrations.** Yeast surface display and titrations were carried out as described (27). Yeast cells (EBY100) containing plasmid encoding the designs were grown overnight at 30 °C in SDCAA medium, inoculated into SGCAA to  $OD_{600}$ , and grown at 22 °C for 16–20 h. Cells were washed once with PBS with 0.1% bovine albumin (PBSF), before adding 700 nM biotinylated IgG (Rituxan) into a total volume of 50  $\mu$ L of the same buffer. Labeling was performed at 4 °C on a rotating platform for 4 h before adding 175 nM streptavidin-PE (Invitrogen) and 4–8  $\mu$ g/mL FITC-labeled anti-Cmyc antibody (ICL Laboratories) for an additional 1 h. Cells were washed once with ice-cold PBSF immediately before measuring their fluorescence via an Accuri C6 flow cytometer; data were analyzed by using the FlowJo 7.6.1 and 8.8.7 software.

**Library Construction.** Random mutagenesis was achieved through a Mutazyme II DNA polymerase kit (Agilent-Stratagene). One hundred nanograms of the FcB6 gene in pETCON were subjected to 31 cycles of amplification with upGS and downCmyc primers (sequences available upon request).

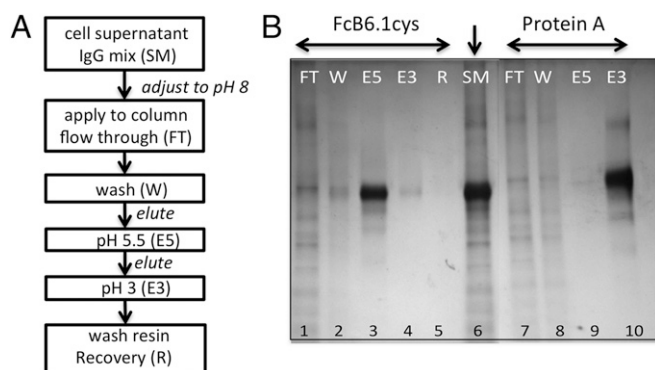


**Fig. 4.** Affinity purification of IgG molecules from cell supernatant. (A) Affinity purification protocol. (B) Purification of human antibody mix from Freestyle 293 suspension cell supernatant. Lanes 1–5, flow through and elution from the FcB6.1cys column; lanes 7–10, flow through and elution on a Protein A column. Lane 6 contains the starting material, the cell supernatant mixed with human antibodies before purification through either column. E3, elution with 100 mM glycine buffer at pH 3; E5, elution with 25 mM phosphate buffer at pH 5.5 and 500 nM NaCl; FT, flow through; R, recovery, wash with TBS; W, wash with TBS.

Mutagenized PCR fragments were cotransformed (28) with linearized pETCON vector (11) into EBY100, resulting in  $1.5 \times 10^8$  variants. Ten individual clones were Sanger sequenced, indicating an average error rate of approximately three nucleotide substitutions per gene. The focused library was constructed through PCR by using ultramer oligonucleotides (IDT dna) with degenerate codons for the variable positions, resulting in two fragments that were cotransformed with linearized plasmid. After transformation into yeast, this library contained  $\sim 5 \times 10^7$  variants.

**Library Selections.** The random mutagenesis library of the original design was incubated while rotating for 4 h at 4 °C with 750 nM biotinylated Rituxan and an additional hour with 187.5 nM streptavidin-PE and 2  $\mu\text{g}/\text{mL}$  anti-myc FITC-labeled antibody producing avid conditions. Cells ( $6.17 \times 10^7$ ) were examined and 106,000 cells were selected by using fluorescence-activated cell sorting on a BD Influx sorter. For the second, focused library, four sorts were performed with 100 nM, 100 nM, 20 nM, and 5 nM biotinylated Rituxan. Cells were incubated in PBSF at indicated pH and above listed Rituxan concentrations at each round of selection, while rotating at 4 °C for 1 h before washing once with 1 mL of ice-cold PBSF. After resuspension in 100  $\mu\text{L}$  of PBSF at corresponding pH levels, 72 nM streptavidin-PE and 2  $\mu\text{g}/\text{mL}$  anti-myc FITC-labeled antibody were added and incubated for an additional 30 min (27) on ice. Detailed information about individual selections are listed in the supplementary material (Figs. S3 and S5).

**Library Preparation and Next-Generation Sequencing.** Plasmids were extracted as described (19). Briefly, approximately  $5 \times 10^7$  cells were treated with Zymolase (50 U) in 400  $\mu\text{L}$  of solution buffer 1 (Zymo Research; yeast plasmid miniprep II) and incubated at 37 °C for 4 h and vortexed every hour. Cells were freeze thawed once and treated as instructed in Zymo kit manual with the exception that lysate was applied to higher-yield columns (QIAGEN; plasmid miniprep kit), followed by plasmid elution with 30  $\mu\text{L}$  of elution buffer (EB) (QIAGEN). Possible contaminating genomic DNA was eliminated through digestion with ExoI (NEB) and Lambda exonuclease (NEB) (19). After a QIAGEN PCR clean-up step, Illumina flow cell adapters and population-specific barcodes were added through PCR (primer sequences available upon request). PCR product was purified through gel extraction (QIAGEN). Spike-in sequencing was done as described by using a HiSeq (Illumina) (19) with appropriate gene-specific sequencing primers (IDT dna). Sequencing reads were split based on their 8-bp barcode into naïve and sorted populations. Pools were treated identically for analysis and quality filtration. Forward and reverse reads with an average phred quality score above 10 were merged into single sequence, in which 49 bp were overlapping; differences between sequences were resolved by using the read information with a higher positional quality score. After quality filtering, 2,894,579 sequences were obtained for the naïve population and 690,046 for the selected pool. Each substitution at each position was counted as a single instance, and the ratio of their frequencies of selected versus unselected populations were computed through custom python and visualized through Mathematica scripts

(available upon request), similarly to previously reported (18, 19). Enrichment values were only plotted if the unselected population had more than 15 occurrences.

**Cloning, Expression, and Purification.** DNA sequences for original designs were synthesized and cloned into pETCON (11) by GenScript USA. FcB6.1 variants were codon optimized by using DNAworks with standard *E. coli* codons and amplified from a gBlock (IDT DNA). Variants were cloned into pET29b by using the NdeI and XhoI sites. Point mutations were generated through overlap PCR, and C-terminal cysteine addition was achieved through an extended primer. Protein variants transformed into BL21(DE3) Star cells were expressed in LB or TB media at 37 °C for 4 or 16 h through induction with 1 mM IPTG. For purification, cells were resuspended in 50 mM Tris, 150 mM NaCl buffer and heated to 80 °C for 20 min, and debris was eliminated through centrifugation. Protein was then applied to a standard Ni column, and buffer exchanged was performed into TBS.

**Binding Analysis.** To obtain a rough estimate for the binding affinity of FcB6.1, an ELISA was performed. FcB6.1 (100  $\mu\text{g}/\text{mL}$ ) in TBS (25 mM Tris at pH 8.2 with 150 mM NaCl) with 1 mM EDTA was coated onto clear 96-well plates overnight at room temperature using 200  $\mu\text{L}$  per well. Plates were blocked with 0.5% (wt/vol) nonfat dried milk (Bio-Rad) in TBS for 2 h. Wells were washed with either TBS at pH 8.2 or PBS (25 mM phosphate buffer at pH 5.5 with 150 mM NaCl) at pH 5.5, and antibody was titrated into the FcB6.1-coated wells in respective buffers. After 45 min, wells were washed two times with appropriate pH-adjusted buffers and containing 0.1% Tween 20, and three times with the same buffers without Tween. After 30-min incubation of Streptavidin-HRP (Bio-Rad) diluted 1:2,000 into either PBS at pH 5.5 or TBS at pH 8, wells were washed as described and incubated shortly with Ultra TMB-Elisa (Thermo Scientific) and quenched with 0.1 M  $\text{H}_2\text{SO}_4$  before measuring absorption at 450 nm. Six independent titrations are reported.

The affinity of the design variants FcB6.1-C132A was determined by using an Octet Red96 (ForteBio). Streptavidin-coated sensors (ForteBio) were coated with 2 nM or 15 nM of biotinylated Rituxan. Binding analysis was performed either in TBS with 0.5% (wt/vol) nonfat dried milk (Bio-Rad) and 0.02% (vol/vol) Tween20 (Sigma-Aldrich) or pH-adjusted PBS with 0.5% (wt/vol) nonfat dried milk (nfdm) and 0.02% (vol/vol) Tween20. All steps were performed at 30 °C while shaking at 1000 rpm (Octet Red96). For regeneration of the sensors, three cycles of alternating for 20 s in 100 mM glycine solution at pH 3 and sodium acetate at pH 5.5 with 0.5% (wt/vol) nfdm were performed. To obtain data for kinetic fits, four titrations at pH 8.2 and pH 5.5 were performed with a shorter association time of 60 s. Global fits of the data using a bivalent ligand model for association and a dissociation time of 120 s were carried out. At pH 8.2, approximately 95% of the response amplitude was associated with a  $K_d$  of  $4.0 (\pm 2.5)$  nM and a second  $K_d$  of  $\sim 13.9$  nM, thus we report 4.0 nM as the main dissociation constant. At pH 5.5, the two averaged  $K_d$  constants from the four titrations were  $5.81 (\pm 1.85)$   $\mu\text{M}$  and  $1.74 (\pm 0.2)$   $\mu\text{M}$ . Because both contribute to the binding signal (70% and 30%), we report their average  $3.78 (\pm 3.2)$   $\mu\text{M}$  as the  $K_d$  value at pH 5.5.

**Resin Coupling.** Purified FcB6.1cys in 25 mM Tris at pH 8.2 was incubated with 25 mM TCEP for at least 1 h at room temperature to reduce possibly disulfide-bonded dimers, followed by the incubation of 4 mg of FcB6.1cys protein per 1 mL SulfoLink resin material (Thermo Scientific) as instructed by the manufacturer's manual. Resin was washed with 10 column volumes of 25 mM Tris at pH 8.2 with 500 mM NaCl and 10 column volumes 25 mM Tris at pH 8.2, followed by incubation with 50 mM cysteine in 25 mM Tris at pH 8.2 and a final wash with TBS.

**IgG Purification.** Twenty micrograms of a human IgG mix (Innovative Research) was spiked into 1 mL of 293 Freestyle suspension cell supernatant. Suspension cells were harvested after 2 wk of expressing an unrelated protein, when the cell density reached  $2\text{--}3 \times 10^6$  cells per mL. To adjust the pH of the supernatant, 10  $\mu\text{L}$  of 1 M Tris at pH 8.2 were added, and the supernatant-IgG mix was incubated while rotating for 30 min at 4 °C. Resin (500  $\mu\text{L}$ ) was allowed to settle and washed with 10 column volumes of TBS at pH 8.2. Antibodies were eluted with 1 mL of 25 mM phosphate buffer with 500 mM NaCl at 5.5, or with 1 mL of 100 mM glycine buffer at pH 3 as indicated on Fig. 3. Fractions eluted with glycine buffer were instantly neutralized by collecting them in tubes containing 200  $\mu\text{L}$  of 1 M Tris at pH 8. For comparison with a Protein A column, Protein A agarose resin was purchased (Pierce), and purification was carried out under the same conditions.

**CD Spectrum.** CD data were collected on an Aviv 420 spectrometer. Far-UV CD wavelength scans (260–200 nm) at 25  $\mu\text{M}$  protein concentration, with either different urea or guanidine hydrochloride concentrations, and temperature ranges (25–95 °C) were collected in a 1-mm path-length cuvette.

**ACKNOWLEDGMENTS.** We thank Nural Orgun and Dr. Oliver W. Press for their donation of Rituxan, Michelle Brault and Dr. David Rawlings for their gift of the Freestyle 293 suspension cell supernatant, Dr. Fabio Parmeggiani for help with CD spectrometer, Dr. Yifan Song for helpful

discussions, and Charlie Lee and Dr. Jay Shendure for running spike-in sequencing reads on their HiSeq Illumina sequencer. The research was supported by the Defense Threat Reduction Agency. S.J.F. was supported by a long-term fellowship from the Human Frontier Science Program.

1. Das R., Morrow KJ (2004) *Antibody Therapeutics: Product Development, Market Trends, and Strategic Issues* (D&MD Publications, Westborough, MA).
2. Kelley B (2009) Industrialization of mAb production technology: The bioprocessing industry at a crossroads. *MAbs* 1(5):443–452.
3. Hristodorov D, et al. (2013) Generation and comparative characterization of glycosylated and aglycosylated human IgG1 antibodies. *Mol Biotechnol* 53(3):326–335.
4. Hari SB, Lau H, Razinkov VI, Chen S, Latypov RF (2010) Acid-induced aggregation of human monoclonal IgG1 and IgG2: Molecular mechanism and the effect of solution composition. *Biochemistry* 49(43):9328–9338.
5. Ejima D, et al. (2007) Effects of acid exposure on the conformation, stability, and aggregation of monoclonal antibodies. *Proteins* 66(4):954–962.
6. Vermeer AW, Norde W (2000) The thermal stability of immunoglobulin: Unfolding and aggregation of a multi-domain protein. *Biophys J* 78(1):394–404.
7. Arakawa T, Philo JS, Tsumoto K, Yumioka R, Ejima D (2004) Elution of antibodies from a Protein-A column by aqueous arginine solutions. *Protein Expr Purif* 36(2):244–248.
8. Tawfik DS, Chap R, Eshhar Z, Green BS (1994) pH on-off switching of antibody-hapten binding by site-specific chemical modification of tyrosine. *Protein Eng* 7(3):431–434.
9. Murtaugh ML, Fanning SW, Sharma TM, Terry AM, Horn JR (2011) A combinatorial histidine scanning library approach to engineer highly pH-dependent protein switches. *Protein Sci* 20(9):1619–1631.
10. Watanabe H, et al. (2009) Optimizing pH response of affinity between protein G and IgG Fc: How electrostatic modulations affect protein-protein interactions. *J Biol Chem* 284(18):12373–12383.
11. Fleishman SJ, et al. (2011) Computational design of proteins targeting the conserved stem region of influenza hemagglutinin. *Science* 332(6031):816–821.
12. Edgcomb SP, Murphy KP (2002) Variability in the pKa of histidine side-chains correlates with burial within proteins. *Proteins* 49(1):1–6.
13. Fleishman SJ, et al. Hotspot-centric de novo design of protein binders. *J Mol Biol* 413(5):1047–1062.
14. DeLano WL, Ultsch MH, de Vos AM, Wells JA (2000) Convergent solutions to binding at a protein-protein interface. *Science* 287(5456):1279–1283.
15. Kuhlman B, et al. (2003) Design of a novel globular protein fold with atomic-level accuracy. *Science* 302(5649):1364–1368.
16. Fleishman SJ, et al. (2011) RosettaScripts: A scripting language interface to the Rosetta macromolecular modeling suite. *PLoS ONE* 6(6):e20161.
17. Du X, et al. (2001) Crystal structure and mechanism of catalysis of a pyrazinamidase from *Pyrococcus horikoshii*. *Biochemistry* 40(47):14166–14172.
18. Fowler DM, et al. (2010) High-resolution mapping of protein sequence-function relationships. *Nat Methods* 7(9):741–746.
19. Whitehead TA, et al. (2012) Optimization of affinity, specificity and function of designed influenza inhibitors using deep sequencing. *Nat Biotechnol* 30(6):543–548.
20. Gao J, Bosco DA, Powers ET, Kelly JW (2009) Localized thermodynamic coupling between hydrogen bonding and microenvironment polarity substantially stabilizes proteins. *Nat Struct Mol Biol* 16(7):684–690.
21. Braisted AC, Wells JA (1996) Minimizing a binding domain from protein A. *Proc Natl Acad Sci USA* 93(12):5688–5692.
22. Schneidman-Duhovny D, Inbar Y, Nussinov R, Wolfson HJ (2005) PatchDock and SymmDock: Servers for rigid and symmetric docking. *Nucleic Acids Res* 33(Web Server issue):W363–367.
23. Lawrence MC, Colman PM (1993) Shape complementarity at protein/protein interfaces. *J Mol Biol* 234(4):946–950.
24. Winn MD, et al. (2011) Overview of the CCP4 suite and current developments. *Acta Crystallogr D Biol Crystallogr* 67(Pt 4):235–242.
25. Cooper S, et al. (2010) Predicting protein structures with a multiplayer online game. *Nature* 466(7307):756–760.
26. Baker NA, Sept D, Joseph S, Holst MJ, McCammon JA (2001) Electrostatics of nano-systems: Application to microtubules and the ribosome. *Proc Natl Acad Sci USA* 98(18):10037–10041.
27. Chao G, et al. (2006) Isolating and engineering human antibodies using yeast surface display. *Nat Protoc* 1(2):755–768.
28. Benatui L, Perez JM, Belk J, Hsieh CM (2010) An improved yeast transformation method for the generation of very large human antibody libraries. *Protein Eng Des Sel* 23(4):155–159.
29. Martin WL, West AP, Jr., Gan L, Bjorkman PJ (2001) Crystal structure at 2.8 Å of an FcRn/heterodimeric Fc complex: Mechanism of pH-dependent binding. *Mol Cell* 7(4):867–877.